Heliyon 8 (2022) e11075

Contents lists available at ScienceDirect

Heliyon

journal homepage: www.cell.com/heliyon

Research article

Fabrication of electrospun *Mondia whitei*/PVA nanofibres: application in the removal of acidic drugs

Ramakwala Christinah Chokwe [a], Temesgen Girma Kebede [a], Simiso Dube [a], Mathew Muzi Nindi [b,*]

[a] *Chemistry Department, Science Campus, University of South Africa, Corner Christiaan De Wet Road and Pioneer Avenue, Florida 1709, South Africa*
[b] *Institute for Nanotechnology and Water Sustainability (iNanoWS), Science Campus, University of South Africa, Corner Christiaan De Wet Road and Pioneer Avenue, Florida 1709, South Africa*

ARTICLE INFO

Keywords:
Mondia whitei
Natural polymer
Mondia whitei/Poly(viny alcohol) blend nanofibres
Adsorption

ABSTRACT

Novel electrospun *Mondia whitei*/PVA blend nanofibres were fabricated for potential water treatment applications by blending a natural polymer extracted from *Mondia whitei* (MW) roots with poly (vinyl alcohol) (PVA). The fabricated nanofibres were shown to have a smooth and uniform morphology with an average diameter of 99 ± 0.025 nm. The FTIR, XPS, XRD, and TGA characterisation results indicated changes in functional groups, crystallinity, and thermal stability of the *Mondia whitei*/PVA blend nanofibres, as compared to the original material. This finding confirmed that the polymers interacted through hydrogen bonding of MW and hydroxyl groups of PVA. The performance of the fabricated nanofibres was investigated for the removal of acidic drugs from spiked water samples. Factors (concentration of acidic drugs, dosage of the nanofibers and contact time) which affect the removal efficiency of the nanofibres were optimised using ultrapure water. Using the nanofibres, 100% removal efficiency for acidic drugs (aspirin, ketoprofen, fenoprofen, diclofenac, and ibuprofen) was achieved. The removal efficiency of the influent wastewater was 76, 89, 97, 93 and 94% for aspirin, ketoprofen, fenoprofen, diclofenac and ibuprofen, respectively, while the removal efficiency of the effluent was 86, 96, 97, 97 and 95% for aspirin, ketoprofen, fenoprofen, diclofenac and ibuprofen, respectively.

1. Introduction

In a world where there is a move towards green chemistry, natural polymers are providing an attractive alternative to synthetic polymers since they are biodegradable and environmentally friendly. Moreover, they are biocompatible and have medicinal properties thus broadening their application scope. New materials that possess properties like high surface area, high tensile strength, conductivity, thermal stability, high functionality, and small diameter are continuously being developed for various applications. Some of these include nanomaterials that are characterised by these attractive properties. Among the nanomaterials, one-dimensional nanofibres have many outstanding features which include superior physicochemical and mechanical performance, together with various morphologies. Due to their advanced characteristics, nanofibers have been applied in various fields such as biomedical, environmental, energy, biotechnology, electronics, and electrical. Electrospinning is one of the methods commonly used for the fabrication of nanofibers due to its simplicity, low cost and high production rate of long and continuous nanofibres, with diameters in the nanometer to micrometer range [1, 2].

Unfortunately, most biopolymers or natural polymers are not spinnable on their own thus necessitating the incorporation of synthetic polymers to improve their spinnability. Synthetic polymers like poly(-vinyl alcohol), poly(lactic acid), poly(glycolic acid), poly(1,4-cyclohexanedimethylene isosorbide terephthalate), and polyethylene oxide are usually blended with natural polymers because of their biodegradability, biocompatibility, water-solubility, and non-toxicity [3, 4, 5, 6].

The concept of polymer blend nanofibres has gained great attention because it results in polymeric materials with improved or modified physicochemical properties. Polymer blends have been reported to exhibit different properties as compared to homopolymers [7]. One of the unique characteristics of polymer blends is the miscibility of the components which controls the physicochemical and mechanical properties, degradation, permeability, and morphology of the nanofibers. Polymer blend nanofibres are made up of structurally distinct polymers that

* Corresponding author.
E-mail address: nindimm@unisa.ac.za (M.M. Nindi).

https://doi.org/10.1016/j.heliyon.2022.e11075
Received 17 June 2022; Received in revised form 15 September 2022; Accepted 10 October 2022

interact via dipole–dipole interaction, charge transfer, and hydrogen bonding with the homopolymer [9, 10]. Some of the polymer blend nanofibres such as chitosan/polyethylene oxide (PEO), *Moringa stenopetala* seed protein/PVA, alginate/soy protein, and cress seed mucilage/PVA, plastic – mimetic polypeptide/polyacrylamide (PAM), Plastic – based polypeptide (PLP)/hydroxypropyl methylcellulose (HPMC), elastin – based polymer/PVA and alginate/PVA have been successfully electrospun and used for the removal of emerging pollutants in environmental water, biomedical application, delivery systems, packaging film fabrication, biotechnological etc. [4, 6, 11, 12, 13, 14, 15, 16, 17, 18]. For example, Paradis-Tanguay et al removed ibuprofen from deionised water using electrospun chitosan/polyethylene oxide (PEO) [4] while Kebede et al removed a group of pharmaceuticals from wastewater using *Moringa stenopetala* seed protein/PVA [19, 20]. *Mondia whitei* has been scientifically studied and reported to have interesting properties that can be explored for application in the medical field such as wound dressing.

Emerging contaminants continue to be topic of interest due to the high volumes of drugs consumed as well as the frequency of detection parent drugs, their metabolites and transformation products. Very few conventional wastewater treatment plants have the capabilities of removing these emerging contaminants from the water. The adsorption method is still regarded as an efficient treatment strategy for organic contaminants and heavy metals in aqueous environments, using different adsorbents. In this work the nanofibres from *M. whitei* root fibres blended with PVA were fabricated, characterised, and applied for the removal acidic drugs from water systems.

2. Experimental

2.1. Chemicals and materials

Formic acid (99%) and polyvinyl alcohol (PVA) with a molecular weight of 89,000–98,000 g mol^{-1} were provided from Sigma-Aldrich (St Louis, USA). All the solutions were made with ultra-pure water (18.2 M) from a Milli-Q® water purification system (Millipore SAS, Molsheim, France). Ketoprofen, diclofenac sodium salt, fenoprofen, ibuprofen and acetylsalicylic acid were supplied by Sigma–Aldrich, were used in the study. The *M. whitei* roots utilized in this study came from KwaZulu-Natal, South Africa.

2.2. Extraction of the polymer from M. whitei roots

A grinder was used to mill the *M. whitei* roots. The fibres were removed from the powder using a sieve, and then digested for 48 h in 99 % formic acid at 80 °C while stirring. To separate the undissolved particles from the extract, the solution was centrifuged. A freeze drier was used to dry the extract (Labconco, USA). Until further use, the freeze-dried powder was kept at room temperature.

2.3. Instrumentation

The Syringe pump (NE-1000 single) supplied by New Era Pump Systems Inc., Farmingdale, NY, USA, was used in the current study. The morphology of the electrospun nanofibres was assessed using the JSM-6010PLUS/LA JEOL-scanning electron microscope fitted with the Oxford X-ray energy dispersive spectroscopy (Rikagu, Japan). An average of 15 SEM images was used to determine the average diameter. The functionalities of the nanofibres were analysed using a Vertex series FTIR spectrometer (Bruker optic GmbH, Hamburg, Germany) coupled with a diamond ATR. The Thermo Scientific K-AlphaTM X Ray Photoelectron Spectrometer (XPS) equipment (Thermo Scientific, Waltham, MA, USA) was used to examine the atomic composition of elements in the materials using monochromatic Al–K radiation. The crystallinity of the MW, and the MW/PVA blend nanofibres was determined with a high resolution SmartLab X-ray diffractometer (XRD) (Rigaku, Japan). The thermal stability of the *M. whitei*/PVA blend nanofibres was assessed using a TGA Q500 Thermogravimetric Analyzer TA Instruments, New Castle, DE, USA). An Agilent 1260 HPLC-DAD system (Waldbronn, Germany) was used to develop the separation method, which consisted of a binary high-pressure pump, auto-sampler, thermostat column compartment, and diode array detector. An XTerra® MS C18 column (4.6 mm × 100 mm, 3.5 μm) (Waters Corporation, Milford, Massachusetts, USA) was used to separate the acidic pharmaceuticals at a temperature of 40 °C, a flow rate of 1.2 mL min^{-1}, and an injection volume of 5 mL. An isocratic elution was carried out with 0.1% formic acid in water (mobile phase A) and acetonitrile (mobile phase B) at a ratio of 48:52 (v/v). The analytes were detected at a wavelength of 230 nm.

2.4. Electrospinning of Mondia whitei blended with PVA

The freeze-dried *Mondia whitei* polymer extract was blended with PVA at different ratios and dissolved in formic acid. As an example, the *Mondia whitei*/PVA blend at a ratio of 70:30 was prepared as follows; 7 g of *Mondia whitei* and 3 g of PVA were mixed and dissolved in 99% formic acid. The mixture was swirled for 2 h on a hot plate at 50 °C to achieve a homogenous mixture, which was then electrospun with a 20 mL disposable syringe. Several parameters were optimised to produce the best nanofibres. The following ratios of *Mondia whitei*/PVA composition were optimised; 20:80, 30:70, 40:60, 50:50, 60:40, 70:30, and 80:20. The polymer concentration was optimised in the range of 7–16% (w/v). The remaining conditions were optimised as follows: voltage: 7.5–20 kV; flow rate: 2.5–10 μL; and tip-to-collector distance: 7.5–17 cm. All the parameters were optimised using the one-at-a-time factor method.

2.5. Adsorption studies

Batch adsorption process were used to determine the removal of acidic drugs using MW/PVA blend nanofibres. The experiments were done by transferring 15 mL of the standard solution to a 25 mL volumetric flask. The nanofibres (i.e., 10–50 mg) were carefully weighed and added to the standard solutions in the flask, which were then well mixed on a water bath shaker before being filtered through a 0.45 m PVDF membrane filter. The dosage, concentration, and time were all optimized by altering one parameter at a time while keeping the others constant. The solutions were then examined using an HPLC-DAD, as detailed in the chromatographic procedures. The equilibrium adsorption capacity of the nanofibres was evaluated using Eq. (1):

$$q_e = \frac{(c_i - c_f)V}{M} \tag{1}$$

and the percentage removal efficiency was calculated using Eq. (2):

$$\%Removal = \frac{(c_i - c_f) * 100}{c_i} \tag{2}$$

where q_e is the amount of acidic drugs adsorbed per unit mass of adsorbent at equilibrium concentration (mg g^{-1}); C_i and C_f are the initial and final concentrations (mg L^{-1}) of acidic drugs, respectively; V is the volume (L) of the adsorption solution; and M is the mass (g) of the adsorbent.

3. Results and discussion

3.1. Effects of polymer solution concentration

The initial parameter to be investigated was concentration of the polymer solution. The concentration of the polymer solution is an important parameter to consider because it influences the electro spinnability and the morphology of the nanofibres produced [2]. At low concentration of the polymer solution, the viscosity of the solution

cannot overcome the surface tension to enable the electrospinning process; this results in spraying of the solution [21]. Nanofibres containing beads are formed when the polymer solution concentration rises until a critical concentration is reached [22]. At higher concentrations, the viscosity of the solution is too high, making it difficult for the solution to be pushed through the needle. In this study, the percentage of the *M. whitei*/PVA blend in formic acid was investigated between 7 and 16%, while keeping the other parameters constant (*M. whitei*/PVA composition at 70:30, flow rate of the solution at 2.5 μL min^{-1}, voltage of 15 kV, and the distance from the tip of the needle to the collector at 12 cm). At a percentage concentration of below 9%, nanofibres with beads were observed and above that concentration, the nanofibres produced were not uniform and were also fracturing (Figure 1a–c). In terms of the diameter of the nanofibres produced, an increase in diameter was observed with an increase in concentration and the average diameter was between 117 and 183 nm (Figure 2(a)). Therefore, 9% was adopted as the optimum/critical concentration to produce nanofibres with an average diameter of 134 nm.

3.2. Effects of M. whitei/PVA composition

The *M. whitei* polymer was blended with polyvinyl alcohol to improve its viscosity and electrospinnability. Ratios of *M. whitei*/PVA ranging from 80:20 to 20:80 (w/w) were investigated as shown in Figure 1 (d–f). All the ratios produced nanofibres without any deformities. The investigating of the diameter of the nanofibres produced using different compositions, it was observed that the nanofibre diameter decreased with an increase of *M. whitei* in the blend as demonstrated in Figure 2(b). Although the nanofibres produced at the 80:20 ratio had a smaller diameter, their size distribution was not as uniform as compared to the 70:30 ratio. Therefore, the *M. whitei*/PVA ratio of 70:30 (w/w) was selected as the optimum with an average nanofibre diameter of 131 nm.

3.3. Effect of solution flow rate and effects of needle tip-to-collector distance

The flow rate of the polymer solution within the needle is important because it determines the polarisability of the solution. Increasing the solution flow rate above the critical value resulted in the nanofibres not drying completely during the electrospinning process, thereby forming beaded nanofibres [22]. This phenomenon was observed in this study at high solution flow rates (>5 μL min^{-1}). At solution flow rates below 5 μL min^{-1} non-uniform nanofibres were produced Figure 1(g–l). Therefore 5 μL min^{-1} was used as the optimum solution flow rate for all the work with an average nanofibre diameter of 89 nm (Figure 2(c)). The phenomenon observed at high flow rates discussed above was similar to the

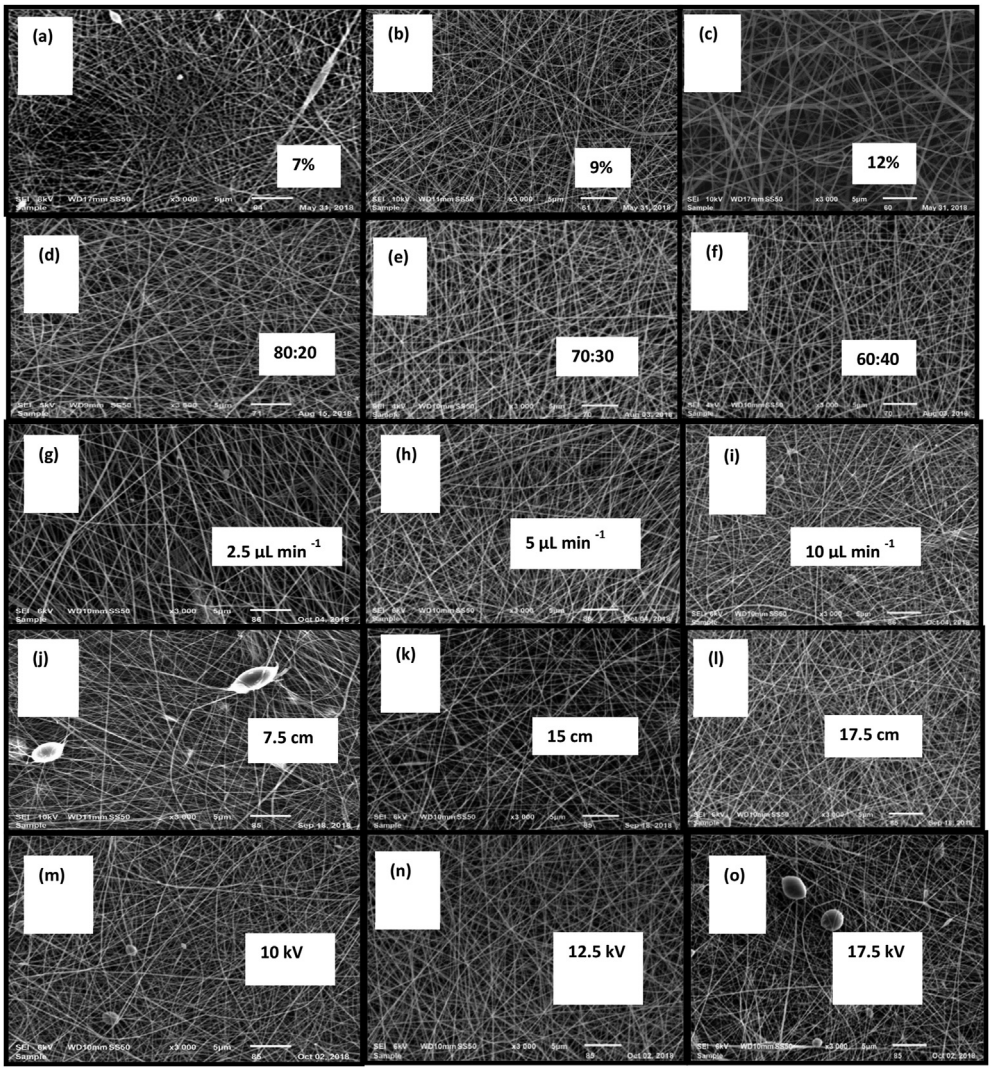

Figure 1. SEM images for optimisation of different electrospinning parameters (a–c: effects of solution concentration; d–f: effects of composition; g–i: effects of solution flow rate; j–l: effects of tip-to-collector distance; and m–o: effects of voltage).

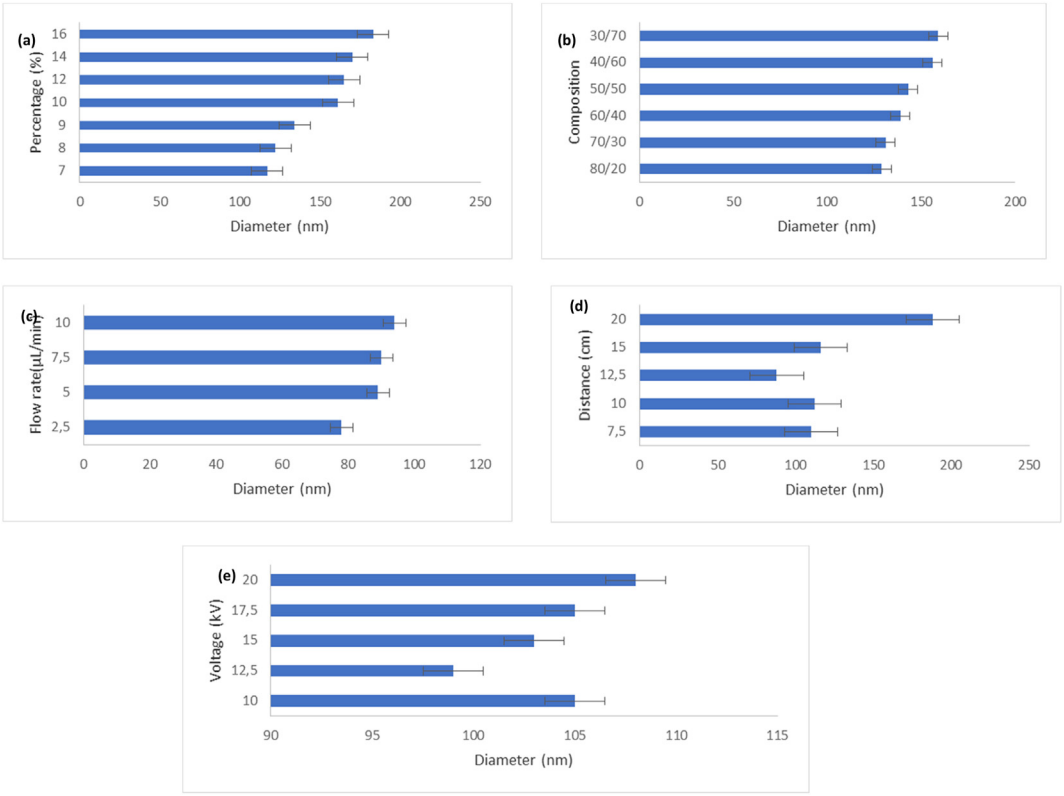

Figure 2. The average diameters of the nanofibres produced under different conditions, 2(a). change in concentrations, 2(b). *M. whitei*/PVA composite, 2(c). change in flow rate, 2(d). needle tip – to-collector distance, 2(e). change in voltage).

effect of shorter distance between the tip of the needle and the collector. In this study, needle tip-to-collector distances ranging from 7.5 to 17.5 cm were investigated. At shorter and longer distances, nanofibres with beads were produced as observed in Figure 1(j–l). At the optimum needle tip-to-collector distance of 15 cm, nanofibres with an average diameter of 116 nm were produced (Figure 2(d)).

3.4. Effects of voltage

The applied voltage can affect both the morphology and diameter of the nanofibres produced. An applied voltage is increased above the critical can result in deformed nanofibres with a large diameter due to the decrease in the size of the Taylor cone. The current study looked at the effect of voltages between 10 and 20 kV while keeping 9% solution concentration, a 70:30 blend composition, a 5 µL min^{-1} solution flow rate, and a 15 cm distance between the needle tip and the collector. It was observed that at low and high voltages (above 12 kV) beaded nanofibres were produced with the latter exhibiting broken nanofibres as shown in Figure 1(m–o). The average nanofibre diameter for the different voltages ranged between 99 and 108 nm as shown in Figure 2(e). The optimum voltage was determined to be 12.5 kV.

3.5. Thermogravimetric analysis (TGA) and differential scanning calorimetry (DSC) of the nanofibres

When a substance is heated or cooled, thermal analysis (thermogravimetric analysis (TGA) and differential scanning calorimetry (DSC)) and differential thermal analysis (DTA) are used to determine the time and temperature at which physical changes occur. Combined thermal analysis (TGA/DSC) provides for the analysis of sample weight loss and heat flow in a single experiment; the device captures TGA weight loss and DSC heat flow data at the same time. The simultaneous thermal analysis (TGA/DSC) results for MW, PVA, and MW/PVA blend nanofibres are given in Figure 3. The effect of heat was assessed by comparison of the degradation temperature of the MW/PVA blend nanofibres with those of *M. whitei* powder and pure PVA nanofibres. As shown in the TGA/DSC curves given for *M. whitei* powder in Figure (3a), the MW powder shows five stages of decomposition. The initial mass loss of the MW powder at a temperature range between 30 and 176 °C is attributed to the evaporation of adsorbed water molecule. The two minor and exothermic peaks (shoulder peaks) over the temperature range 224–282 °C (DSC) could be due to the decomposition of low-temperature volatile compounds and monosaccharide rings. This is followed by a severe mass loss shown by peaks at around 306 °C and the fifth stage at 498 °C; these could be due to the decomposition and disintegration of macromolecular chains of the polymer. The exothermic peak at the temperature of 836 °C (DSC) could be due to the presence of impurities. The thermal stability of pure PVA nanofibres was also tested as a reference. As presented in Figure 3b (TGA/DSC curves for PVA), the mass loss curve as a function of temperature shows levels of the degradation. The first stage of the PVA mass loss curve was between 30 and 250 °C, attributed to the loss of moisture, physisorbed and chemisorbed water molecules [23], with a mass loss of 8%; the second and third major mass loss of approximately 82% was observed at the exothermic peak between 301 and 444 °C, related to the degradation of the PVA side chains [24]. Finally, the stage at around 506 °C corresponds to the complete decomposition of the main PVA chain, leaving a small amount of residue [25].

The thermal degradation profile of the MW/PVA blend nanofibres indicated four main decomposition stages. The first stage can be attributed to the loss of moisture that started at around 214 °C. Typically, the water loss above 100 °C was related to the evaporation of water entrapped among the chains of MW/PVA blend nanofibres. The major peak observed on the DSC curve at around 306 °C with weight loss of 30% is probably due to the degradation of the monosaccharide rings of the MW/PVA blend nanofibres. The third and fourth stages of degradation were observed on the DSC curve at temperatures of 348 and 433 °C

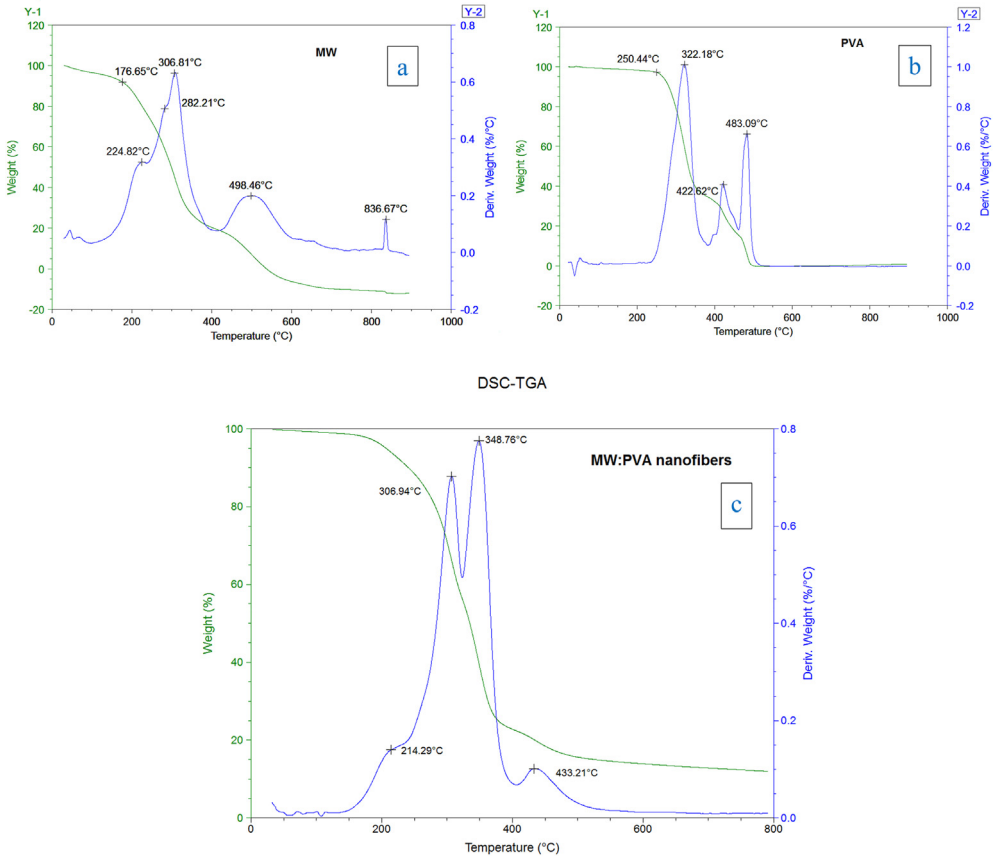

Figure 3. Thermal analysis of the three materials: TGA/DSC curves for MW(a), PVA(b), and MW/PVA(c) blend nanofibres (blue line for DSC curve; and black line for TGA curve).

with the mass loss of about 60 and 79%, respectively. This decomposition could be due to the complete disintegration of the MW/PVA blend nanofibres with small amounts of residues. If there is no interaction between these two polymers, the thermogram of the blends will indicate its heat degradation in eight or more phases. However, as shown in Figure 3c, each of the MW/PVA blend nanofibres only has four stages of degradation. These results indicated that the degradation stages are completely different from the original materials, namely pure PVA and MW. As an example, the first stage of decomposition for the MW/PVA blend nanofibres started at 214 °C and at 176 °C and 250 °C for the pure MW and PVA, respectively. This indicated the presence of hydrogen bonding interactions between MW and PVA in each blend. The bonding occurs through COOH/NH group of MW and OH group of PVA. From the results, it was also observed that the introduction of PVA in the blend increased the thermal stability of the MW/PVA blend nanofibres. The results indicated that these two polymers are well blended together.

3.6. FTIR analysis of the pure MW and PVA nanofibres and MW/PVA blend nanofibres

Figure 4 shows the characteristic functional groups of pure MW and PVA nanofibres, and MW/PVA blend nanofibres. Table 1 shows the absorption bands and their corresponding functionalities of pure MW and PVA nanofibers.

Compared to the FTIR spectra of the pure MW and PVA, a difference was observed in the spectrum of the MW/PVA blend nanofibres. The absorption bands at 3 251 cm^{-1} and 3 340 cm^{-1} due to –OH stretching vibration and –NH vibration of pure PVA and MW are shifted to a higher wave number (3 402 cm^{-1}) for the MW/PVA blend nanofibres. Additionally, changes in the intensity and position of the peaks were observed from wave numbers of 1 515, 1 240 and 1 170 cm^{-1} for MW, and 1 527, 1

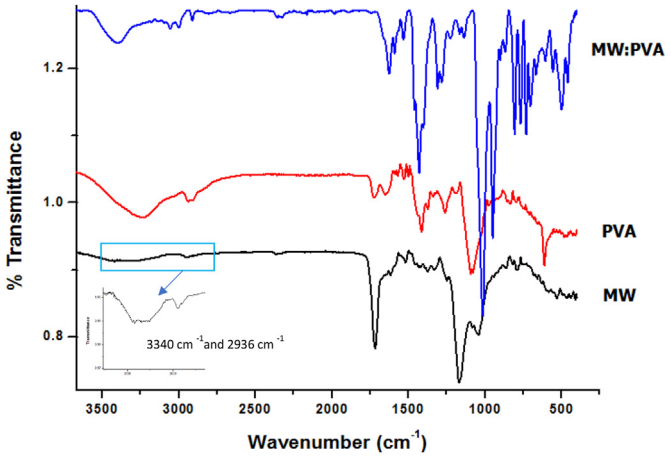

Figure 4. FTIR spectra of MW and PVA nanofibres and MW/PVA blend nanofibres.

413, 1 093 and 1 073 cm^{-1} for pure PVA, to wave numbers of 1 534, 1 432, 1 281, 1 166 and 1 133 cm^{-1} for the MW/PVA blend nanofibres. In the FTIR spectrum of the MW/PVA blend nanofibres, the absorption bands observed for the pure MW and PVA at 1 715 cm^{-1} and 1 717 cm^{-1}, respectively, have disappeared. Moreover, new IR bands appeared in the spectrum of the MW/PVA blend nanofibres at 1 625, 1 587, 1 462, 1 313, 1 014, and 949 cm^{-1}. This shows how the physico-chemical interactions of different polymers in a blended mixture can alter the characteristic peaks of the spectrum. Therefore, all the changes on the characteristic peaks confirmed the complete miscibility between the MW and the PVA.

Table 1. Pure MW and PVA nanofibers absorbance bands and their associated functional groups.

	Absorption	MW	PVA nanofibers	Group	References
1	3340 cm^{-1}	yes	-	N–H vibration	
2	2936 cm^{-1}	yes	-	C–H	
3	1717 cm^{-1}	yes	-	C=O	
4	1440 cm^{-1}	yes	-	O–H stretching	
5	1372 cm^{-1}	Yes	-	C–O in plane stretching vibration	[26]
6	1240 cm^{-1}	yes	-	C(O)–O stretching (ester group)	[27]
7	1170 cm^{-1}	yes	-	C–O stretching	[28]
8	1021 cm^{-1}	yes	-	C–O stretching vibration	
9	3251 cm^{-1} and 1425 cm^{-1}		yes	O–H (hydroxyl group)	
10	2936 cm^{-1} and 2899 cm^{-1}		yes	CH_2 symmetric and asymmetric stretching vibration	
11	1715–1564 cm^{-1}		yes	C = C stretching vibration	
12	1145 cm^{-1}		yes	CH–OH bending	
13	1313 cm^{-1}		yes	CH_2 waging	
14	1236 cm^{-1}		yes	CH waging	
15	1137 cm^{-1}		yes	C–O–C stretching	[29]
16	1093–898 cm^{-1}		yes	C–C stretching	[30, 31]

The most probable interaction between the MW and the PVA is hydrogen bonding/peptide bond linkage through COOH and NH functional groups of MW and –OH of PVA.

3.7. XRD analysis of pure MW, PVA, and MW/PVA blend nanofibres

The crystallinity of pure MW, PVA, and MW/PVA blend nanofibres was analysed using XRD. The XRD patterns of pure MW, PVA, and MW/PVA blend nanofibres are shown in Figure 5. The pure MW XRD pattern has three peaks at $2\theta = 8.8°$, 10.6°, and 20.94°. These are an indication of the different crystalline nature of the pure MW powder. From the XRD patterns of PVA nanofibres, two peaks were observed at $2\theta = 10.8°$ and 19.6°. The sharp peak at $2\theta = 19.6°$ shows the degree of crystallinity of PVA. Similar results were reported by M. Koosha, and H. Mirzadeh and

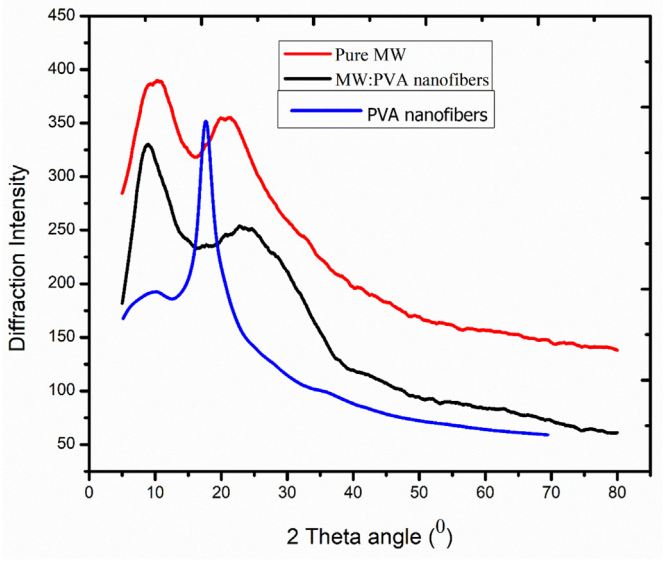

Figure 5. The XRD patterns of pure MW, PVA, and MW/PVA blend nanofibres.

Kebede et al. [6, 32]. From the XRD patterns of the MW/PVA blend nanofibres, it is observed that the nanofibres synthesised from the blend are more amorphous than those in the raw materials. Some of the changes included the shift in the peak positions and disappearance of the peak. For example, for pure PVA and MW, the peaks at $2\theta = 19.65°$, 10°, 19°, and at $2\theta = 20.94°$, 9.7° are now transformed to peak position $2\theta =$ 23.87° and 8.94° in the MW/PVA blend nanofibres. The peak at $2\theta =$ 10.19° of the MW powder disappeared as compared to the MW/PVA blend nanofibres. In comparison to PVA, the crystallinity of the synthesised nanofibres is altered. This could be due to the electrospinning process. In this process, the electric field is used to elongate the jet and concurrently the solvent is evaporated rapidly to produce the nanofibres The electrospinning method may have impeded crystallisation of the MW/PVA blend nanofibres by interfering with the development of crystalline microstructures inside the material. During electrospinning, the rapid solidification of the stretched molecular chains at very high elongation rates significantly hinders the formation of crystal structures in nanofibres. Through elongation, the diameter of the jet is reduced, and the solvent (small molecule) evaporates instantly, while macromolecules such as polymer chains, take longer to disperse and rearrange into crystals. The jet solidifies in a fraction of a second, whereas crystallisation from a semi-dilute polymer solution takes days. The time required for solvent evaporation was less than the time required for crystal formation. As a result, the degree of crystallinity in the electrospun nanofibres is very low, and the majority of the polymer chains are in an amorphous phase). These results also confirm the interaction of PVA with MW via hydrogen bonding and peptide bond linkage, as observed in the FTIR data (Figure 4).

3.8. XPS analysis of MW, and MW/PVA blend nanofibres

The most common technique for evaluating the atomic elemental composition and chemical changes on a material surface is XPS. Figure 6a shows the full scan of the raw (pure) MW and MW/PVA blend nanofibres. The XPS results of the raw (pure) MW (Figure 6a) showed that there are four primary peak components, each with a different binding energy (eV). The peaks at 284.2 eV, 284.9 eV, 286.1 eV, 288.0 eV, and 288.7 eV are respectively assigned to C–C sp^2, C–C sp^3, C–O, C=O, and O–C=O (Figure 6b). In addition, the peaks at 400.1 eV, 531.7 eV, 533.1 eV, and 688.3 eV are attributed to N (Figure 6f), C–O (O1s), C=O (O1s) (Figure 6d) and F (Figure 6h), respectively. Three major peaks are observed for the MW/PVA blend nanofibres (Figure 6a). The peaks at 284.2 eV, 284.6 eV, 286.2 eV, 287.5 eV, and 288.8 eV correspond to C–C sp^2, C–C sp^3, C–O, C=O and O–C=O (Figure 6c), while peaks at 399.7 eV, 531.9 eV, and 533.0 eV are attributed to N (Figure 6g), C–O (O 1s) and C=O (O 1s) (Figure 6e). The atomic composition of N in the produced MW/PVA blend nanofibres was considerably reduced (from 17.5 to 0.6% (Table 1)) at 531.7 eV, with disappearing peaks at 688.3 corresponding to F. Furthermore, the atomic composition of C in the synthesised nanofibres is higher than that of the raw MW, as shown in Table 2. These results confirmed that there was a possible interaction between MW and PVA through hydrogen bonding using the amine functional group ($–NH_2$) of MW and the carboxyl functional group (–COOH) of PVA). This finding is also consistent with FTIR results, which show that the absorption band at 3340 cm^{-1} (due to amine groups of MW) disappears once the polymer blend nanofibres have been synthesised.

4. Adsorption of acidic drugs using the *M. whitei*/PVA blend nanofibres

4.1. Optimisation of parameters that can affect the removal process

It is necessary to optimise parameters which significantly affect the adsorption efficiency of the nanofibres to achieve the maximum possible percentage removal. Such parameters which include dosage,

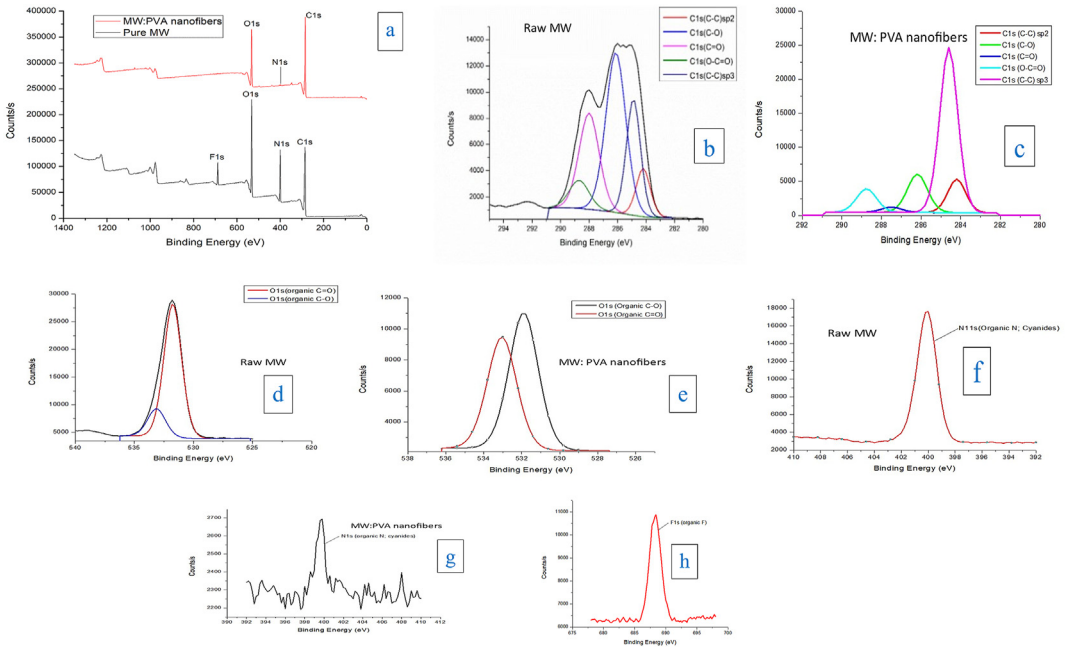

Figure 6. The XPS analysis of raw MW and MW/PVA blend nanofibres (6a), carbon of raw MW (6b), carbon of MW/PVA nanofibers (6c), oxygen of raw MW (6d), oxygen of MW/PVA nanofibers (6e), nitrogen of raw MW (6f), nitrogen of raw MW/PVA nanofibers (6g) and fluorine of raw MW (h).

Table 2. Atomic composition and elemental ratios analysed by XPS for MW powder and MW/PVA blend nanofibres.

Sample	Atomic composition (%)			
	C	O	N	F
Raw MW	56.7	21.8	17.5	4.0
MW/PVA blend nanofibres	76.4	21.7	0.6	-

concentration, and time were optimised. After each optimisation step, the removal efficiency was calculated, and the optimum condition was selected.

4.1.1. Percentage adsorption at different analyte concentrations

The removal efficiency of adsorbent is greatly influenced by the concentration of the adsorbate. The percentage removal reduces as the concentration of analytes increases. This could be because the concentrations of the analytes determine the number of molecules attached to the active sites of the adsorbent (nanofibers). There will be a significant percentage removal at lower concentrations, which could be attributable to the availability of adequate active sites on the nanofibers surface. As shown in Figure 7, an increase in the initial concentration of acidic drugs led to drop in the percentage removal. This could be due to the acid drug molecules occupying all of the accessible active sites on the nanofibre surface, leaving no more sites available for subsequent adsorption. The maximum possible removal is ranged from 50.9 to 89.4% for all analytes at a dosage of 10 mg, concentration of 0.5 mg L^{-1}, volume of 25 mL, contact time of 30 min, and agitation speed of 100 rpm.

4.1.2. Percentage adsorption at different contact times

Figure 8 shows the influence of contact time on the adsorption of acidic drugs from aqueous solution. The percentage removal changed as the contact time extended from 10 to 30 min, as observed in the results. The adsorption of acidic drugs using the MW/PVA blend nanofibres showed a slight increase with an increase in contact time from 30 to 60 min. Owing to the rapid exhaustion of adsorption sites, extending the contact time did not result in any meaningful changes. This implies that the adsorption was very fast and reaches equilibrium at 60 min. This phenomenon could be explained by the availability of active sites on the surface of the MW/PVA blend nanofibres for the rapid adsorption of acidic drugs. The maximum percentage adsorption at 60 min was found to be in the range of 84.5–97.4%. Therefore, 60 min was selected as the optimum time.

4.1.3. Percentage adsorption at different nanofibre dosages

As illustrated in Figure 9, the adsorbent dosage is clearly a significant parameter that determines the adsorption process. The percentage adsorption of the nanofibres was examined at various adsorbent dosages, ranging from 10 mg to 50 mg, while all other parameters remained constant. Since the percentage adsorption is dependent on the average active site of the adsorbent, as the adsorbent dosage increases consequently the percentage adsorption of acidic drugs was also increased. From the result obtained, it was observed that at an adsorbent dosage of 50 mg, the maximum possible removal was achieved for all analytes. At a nanofibre dosage of 50 mg, 100% adsorption was observed for all acidic drugs.

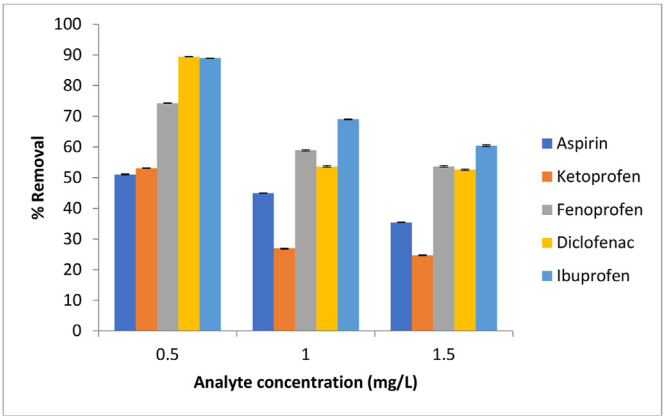

Figure 7. Effect of analyte concentration on the adsorption of acidic drugs.

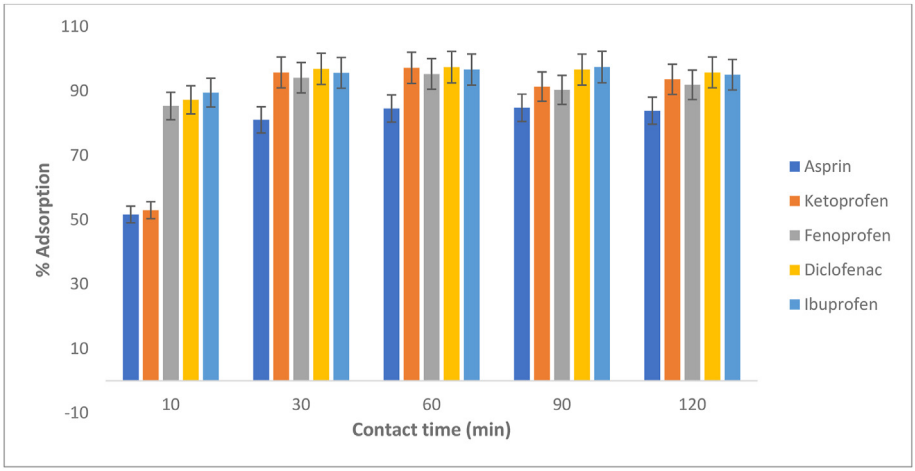

Figure 8. Contact time Vs percentage removal of acidic drugs.

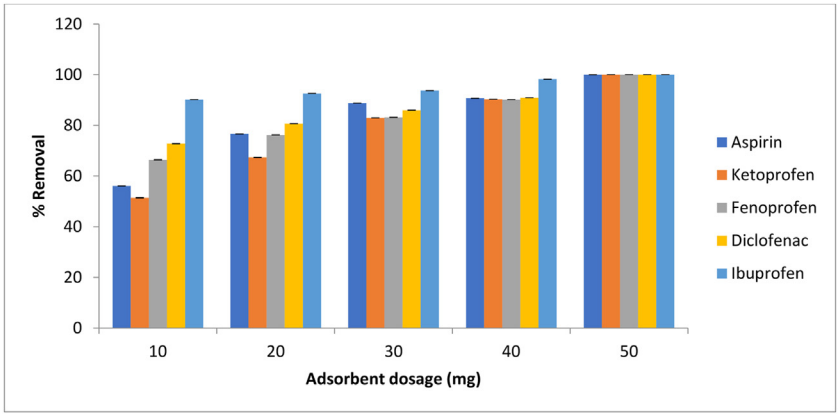

Figure 9. Effect of nanofibre dosage on the adsorption of acidic drugs.

5. Application of nanofibres for treatment of wastewater (influent and effluent)

The nanofibres were applied to both influent and effluent wastewater spiked with the five acidic drugs of interest for their removal. The removal efficiency of the influent wastewater was 76, 89, 96, 93 and 94% for aspirin, ketoprofen, fenoprofen, diclofenac and ibuprofen, respectively, While the removal efficiency of the effluent was 86, 96, 97, 97 and 95% for aspirin, ketoprofen, fenoprofen, diclofenac and ibuprofen, respectively (Figure 10).

As compared with materials used for the removal of selected drugs, MW/PVA nanofibers emerged as a viable alternative for usage in water treatment. For example, Adityosulindro and co-workers reported inefficient removal of ibuprofen from wastewater and deionised water (24% and 48 %, respectively), using sonolysis and sono-Fenton oxidation [33]. Song et al. reported 11%, 42% and 70% removal of diclofenac using

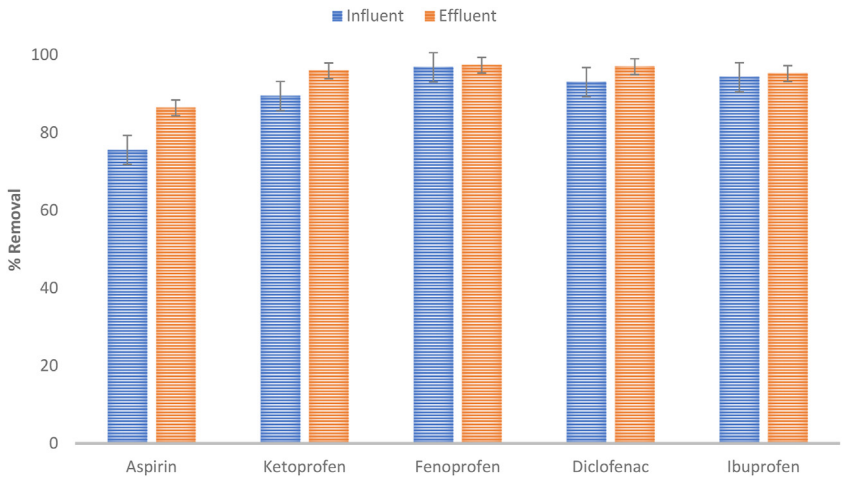

Figure 10. Application of nanofibres on real wastewater samples (influent and effluent).

modified nanoscale zerovalent iron (nZVI, Ni – nZVI and Sn – nZVI, respectively) from simulated ground water [34]. In the study reported by ALOthman et al., 89% of ketoprofen was removed from distilled water using copper nanoparticles [35]. Niragire et al. used Chitosan/PVA nanofibers to study the removal of acetyl salicylic acid and fenoprofen (100%); however, the removal efficiency was greatly impacted since the nanofibers were applied to wastewater (effluent), and the results reported were 40.8% and 59%, respectively [36].

6. Mechanism of the adsorption

The MW/PVA nanofibers contain a diversity of functional groups since they were made from a material with a variety of functional groups. In comparison to MW, which mostly comprises –NH and COOH groups, PVA has functional groups such as C–H (saturated hydrocarbons), C–O (alcohol group), C=O (carbonyl group), and O–C=O (carboxylate group). According to the FTIR data, the synthesized MW/PVA nanofibers contained functional groups such C–H, –NH, C = C, C(O)–O, C–O, and C–O–H. According to the XPS data, the MW/PVA nanofibers comprise functional groups including C–C, C–O, O–C–O, N, and C=O. These functional groups are primarily control of any potential interactions between acidic drugs and MW/PVA nanofibers in different water systems. It is possible to infer from the findings that the nanofibers are likely to interact with the acidic drugs through electrostatic interaction, H-bonding or π-π interaction.

7. Conclusions

Mondia whitei root extract was successfully blended with PVA and electrospun to produce smooth and uniform nanofibres with an average diameter of 98–105 ± 0.025 nm. The concentration of the polymer solution was found to be the most important factor in the fabrication nanofibers from blended polymer solutions, as presented in SEM images. The polymer composition (MW:PVA, 20:80–20:80) had no effect on the nanofibre morphology except that the diameter increased with an increase in PVA. The nanofibres were mainly characterised by hydroxyl and carboxylic groups. Blending resulted in nanofibres with improved thermal stability. Application of the nanofibres under optimum conditions resulted in 100%, 97% and 96% removal efficiency of acidic drugs from spiked UHP water and wastewater (influent and effluent), respectively. The MW/PVA blend nanofibres were shown to be potential alternative adsorbents for the removal of acidic drugs from water.

Declarations

Author contribution statement

Ramakwala Christinah Chokwe, Temesgen Girma Kebede: Conceived and designed the experiments; Performed the experiments; Analyzed and interpreted the data; Wrote the paper.

Simiso Dube, Mathew Muzi Nindi: Contributed reagents, materials, analysis tools or data.

Funding statement

This research did not receive any specific grant from funding agencies in the public, commercial, or not-for-profit sectors.

Data availability statement

Data will be made available on request.

Declaration of interests statement

The authors declare no conflict of interest.

Additional information

No additional information is available for this paper.

Acknowledgements

The authors are appreciative to the University of South Africa, Department of Chemistry for assisting them with this study by providing the necessary resources.

References

[1] A. Haider, S. Haider, I.K. Kang, A comprehensive review summarizing the effect of electrospinning parameters and potential applications of nanofibers in biomedical and biotechnology, Arab. J. Chem. 11 (2015) 1165–1188.

[2] A. Greiner, J.H. Wendorff, Electrospinning: a fascinating method for the preparation of ultrathin fibers, Angew. Chem. Int. Ed. 46 (2007) 5670–5703.

[3] M.Q. Khan, H. Lee, Z. Khatri, D. Kharaghani, M. Khatri, T. Ishikawa, S.S. Im, I.S. Kim, Fabrication and characterization of nanofibers of honey/poly(1,4-cyclohexane dimethylene isosorbide terephthalate) by electrospinning, Mater. Sci. Eng. C 81 (2017) 247–251.

[4] L. Paradis-Tanguay, A. Camiré, M. Renaud, B. Chabot, A. Lajeunesse, Sorption capacities of chitosan/polyethylene oxide (PEO) electrospun nanofibers used to remove ibuprofen in water, J. Polym. Eng. 39 (2018) 207–215.

[5] Y.T. Jia, J. Gong, X.H. Gu, H.Y. Kim, J. Dong, X.Y. Shen, Fabrication and characterization of poly (vinyl alcohol)/chitosan blend nanofibers produced by electrospinning method, Carbohydr. Polym. 67 (2007) 403–409.

[6] T.G. Kebede, S. Dube, M.M. Nindi, Fabrication and characterization of electrospun nanofibers from *Moringa stenopetala* seed protein, Mater. Res. Express 5 (2018), 125015.

[7] M.S. Islam, M.R. Karim, Fabrication and characterization of poly(vinyl alcohol)/alginate blend nanofibers by electrospinning method, Colloids Surfaces A Physicochem. Eng. Asp. 366 (2010) 135–140.

[9] E.M. Woo, J.W. Barlow, D.R. Paul, Phase behavior of blends of aliphatic polyesters with a vinylidene chloride/vinyl chloride copolymer, J. Appl. Polym. Sci. 32 (1986) 3889–3897.

[10] D.F. Varnell, J.P. Runt, M.M. Coleman, FT-IR. and thermal analysis studies of blends of poly(ε-caprolactone) with homo- and copolymers of poly(vinylidene chloride), Polymer (Guildf). 24 (1983) 37–42.

[11] R. Wongkanya, P. Chuysinuan, C. Pengsuk, S. Techasakul, K. Lirdprapamongkol, J. Svasti, P. Nooeaid, Electrospinning of alginate/soy protein isolated nanofibers and their release characteristics for biomedical applications, J. Sci. Adv. Mater. Dev. 2 (2017) 309–316.

[12] A. Fahami, M. Fathi, Fabrication and characterization of novel nanofibers from cress seed mucilage for food applications, J. Appl. Polym. Sci. 135 (2018) 4–9.

[13] G.S. Nanjundaswamy, B. Mahesh, G.D. Channe Gowda, N.A. Chamaraja, A. Gangadhar, Examination of miscibility characteristics of the synthetic plastic-mimetic peptide with polyacrylamide: development of nonwoven mats by electrospinning, Polym.-Plast. Technol. Mater. 60 (4) (2021) 405–418.

[14] B. Mahesh, D. Kathyayani, G.S. Nanjundaswamy, D. Channe Gowda, R. Sridhar, Miscibility studies of plastic-mimetic polypeptide with hydroxypropylmethylcellulose blends and generation of non-woven fabrics, Carbohydr. Polym. 212 (2019) 129–141.

[15] N.G. Siddamallappa, M. Basavaraju, C.G. Dase Gowda, Elastin-based polymer: synthesis, characterization and examination of its miscibility characteristics with poly(vinyl alcohol) and electrospinning of the miscible blends, Polym. Int. 67 (11) (2018) 1511–1522.

[16] A. Partovinia, M. Koosha, Fabrication of novel nanocomposite nanofibrous matrices retaining high concentration of microbial cells for heavy crude oil biodegradation, Express Polym. Lett. 13 (5) (2019) 484–499.

[17] M.S. Islam, M.R. Karim, Fabrication and characterization of poly(vinyl alcohol)/alginate blend nanofibers by electrospinning method, Colloids Surf. A Physicochem. Eng. Asp. 366 (1–3) (2010) 135–140.

[18] M. Rafienia, A. Saberi, E. Poorazizi, A novel fabrication of PVA/Alginate-Bioglass electrospun for biomedical engineering application, Nanomed. J. 4 (3) (2017) 152–163.

[19] T.G. Kebede, S. Dube, M.M. Nindi, Removal of non-steroidal anti-inflammatory drugs (NSAIDs) and carbamazepine from wastewater using water-soluble protein extracted from *Moringa stenopetala* seeds, J. Environ. Chem. Eng. 6 (2018) 3095–3103.

[20] T.G. Kebede, S. Dube, M.M. Nindi, Biopolymer electrospun nanofibres for the adsorption of pharmaceuticals from water systems, J. Environ. Chem. Eng. 7 (2019), 103330.

[21] J.M. Deitzel, J. Kleinmeyer, D. Harris, N.C. Beck Tan, The effect of processing variables on the morphology of electrospun nanofibers and textiles, Polymer (Guildf) 42 (2001) 261–272.

[22] Z. Li, C. Wang, One-Dimensional Nanostructures: Electrospinning Technique and Unique Nanofibers, in: Book Series: SpringerBriefs in Materials, 2013.

[23] R. Anbarasan, R. Pandiarajaguru, R. Prabhu, V. Dhanalakshmi, A. Jayalakshmi, B. Dhanalakshmi, S. Ulfath Nisha, S. Gandhi, T. Jayalakshmi, Synthesis,

characterizations, and mechanical properties of structurally modified poly(vinyl alcohol), J. Appl. Polym. Sci. 117 (2010) 2059–2068.
[24] B.J. Holland, J.N. Hay, The thermal degradation of poly(vinyl alcohol), Polymer (Guildf). 42 (2001) 6775–6783.
[25] G. Kim, Y. Hwang, Y. Ahn, H. Shin, J. Lee, C. Sung, The morphology of electrospun polystyrene fibers, Kor. J. Chem. Eng. 22 (2005) 147–153.
[26] S. Felhi, M. Saoudi, A. Daoud, H. Hajlaoui, M. Ncir, R. Chaabane, A. El Feki, N. Gharsallah, A. Kadri, Investigation of phytochemical contents, in vitro antioxidant and antibacterial behavior and in vivo anti-inflammatory potential of *Ecballium elaterium* methanol fruits extract, Food Sci. Technol. 37 (2017) 558–563.
[27] S. Paszkiewicz, A. Szymczyk, D. Pawlikowska, I. Irska, I. Taraghi, R. Pilawka, J. Gu, X. Li, Y. Tu, E. Piesowicz, Synthesis and characterization of poly(ethylene terephthalate-*co*-1,4-cyclohexanedimethylene terephthalate)- *block* -poly(tetramethylene oxide) copolymers, RSC Adv. 7 (2017) 41745–41754.
[28] S. Balamurugan, A.R. Balu, K. Usharani, M. Suganya, S. Anitha, D. Prabha, S. Ilangovan, Synthesis of CdO nanopowders by a simple soft chemical method and evaluation of their antimicrobial activities, Pacific Sci. Rev. A Nat. Sci. Eng. 18 (2016) 228–232.
[29] S. Krimm, C.Y. Liang, G.B.B.M. Sutherland, Infrared spectra of high polymers. V. Polyvinyl alcohol, J. Polym. Sci. 22 (1956) 227–247.
[30] N. El Miri, K. Abdelouahdi, M. Zahouily, A. Fihri, A. Barakat, A. Solhy, M. El Achaby, Bio-nanocomposite films based on cellulose nanocrystals filled polyvinyl alcohol/chitosan polymer blend, J. Appl. Polym. Sci. 132 (2015) 1–13.
[31] J. Bonilla, E. Fortunati, L. Atarés, A. Chiralt, J.M. Kenny, Physical, structural and antimicrobial properties of poly vinyl alcohol-chitosan biodegradable films, Food Hydrocolloids 35 (2014) 463–470.
[32] M. Koosha, H. Mirzadeh, Electrospinning, mechanical properties, and cell behavior study of chitosan/PVA nanofibers, J. Biomed. Mater. Res., Part A 103 (2015) 3081–3093.
[33] S. Adityosulindro, L. Barthe, K. González-Labrada, U.J. Jáuregui Haza, H. Delmas, C. Julcour, Sonolysis and sono-Fenton oxidation for removal of ibuprofen in (waste) water, Ultrason. Sonochem. 39 (2017 Nov 1) 889–896.
[34] S. Song, Y. Su, A.S. Adeleye, Y. Zhang, X. Zhou, Optimal design and characterization of sulfide-modified nanoscale zerovalent iron for diclofenac removal, Appl. Catal., B 201 (2017) 211–220.
[35] Z.A. ALOthman, A.Y. Badjah, O.M. Alduhaish, K. Rathinam, S. Panglisch, I. Ali, Synthesis, characterization, kinetics and modeling studies of new generation pollutant ketoprofen removal in water using copper nanoparticles, J. Mol. Liq. (2021) 323.
[36] H. Niragire, T.G. Kebede, S. Dube, M. Maaza, M.M. Nindi, Chitosan-based electrospun nanofibers mat for the removal of acidic drugs from influent and effluent, Chem. Eng. Commun. (2022) 1–23.